

# ORMNet: Object-centric Relationship Modeling for Egocentric Hand-object Segmentation

Yuejiao Su, Yi Wang, *Member, IEEE*, and Lap-Pui Chau, *Fellow, IEEE*

**Abstract**—Egocentric hand-object segmentation (EgoHOS) is a brand-new task aiming at segmenting the hands and interacting objects in the egocentric image. Although significant advancements have been achieved by current methods, establishing an end-to-end model with high accuracy remains an unresolved challenge. Moreover, existing methods lack explicit modeling of the relationships between *hands and objects* as well as *objects and objects*, thereby disregarding critical information on hand-object interaction and introducing confusion into algorithms, ultimately leading to a reduction in segmentation performance. To address the limitations of existing methods, this paper proposes a novel end-to-end Object-centric Relationship Modeling Network (ORMNet) for EgoHOS. Specifically, based on a single-encoder and multi-decoder framework, we design the Hand-Object Relation (HOR) module to leverage hand-guided attention to capture the correlation between hands and objects and facilitate their representations. Moreover, based on the observed interrelationships between diverse categories of objects, we introduce the Object Relation Decoupling (ORD) strategy. This strategy allows the decoupling of the two-hand object during training, thereby alleviating the ambiguity of the network. Experimental results on three datasets show that the proposed ORMNet has notably exceptional segmentation performance with robust generalization capabilities.

**Index Terms**—Egocentric view, hand-object interaction segmentation, attention, relationship modeling.

## I. INTRODUCTION

THE advancements in edge computing and computer vision have engendered a growing interest in Head-Mounted Devices (HMD) such as the Apple Vision Pro [1] and Microsoft Hololens 2 [2]. Consequently, there is a rising trend in capturing abundant first-person view (FPV) or egocentric images and videos. Compared with data captured from a third-person view (TPV) or an exocentric perspective [3], egocentric data displays the actions and intentions of the HMD wearer more clearly and intuitively, which is more conducive to analyzing human behavior and understanding how humans interact with the environment. Notably, questions concerning the activities of individuals, such as “*What is this person doing?*” can be more comprehensively addressed through the parsing of egocentric visual data. It is obvious that the hands of HMD wearers and the objects they are interacting with serve as pivotal cues in this analysis.

Therefore, to delve deeply into human behavior encoded within egocentric data at a fine-grained level, Zhang *et al.* [4] first proposed the Egocentric Hand-Object Segmentation

Yuejiao Su, Yi Wang, and Lap-Pui Chau are with the Department of Electrical and Electronic Engineering, The Hong Kong Polytechnic University, Hong Kong SAR (e-mail: yuejiao.su@connect.polyu.hk; yi-eie.wang@polyu.edu.hk; lap-pui.chau@polyu.edu.hk).

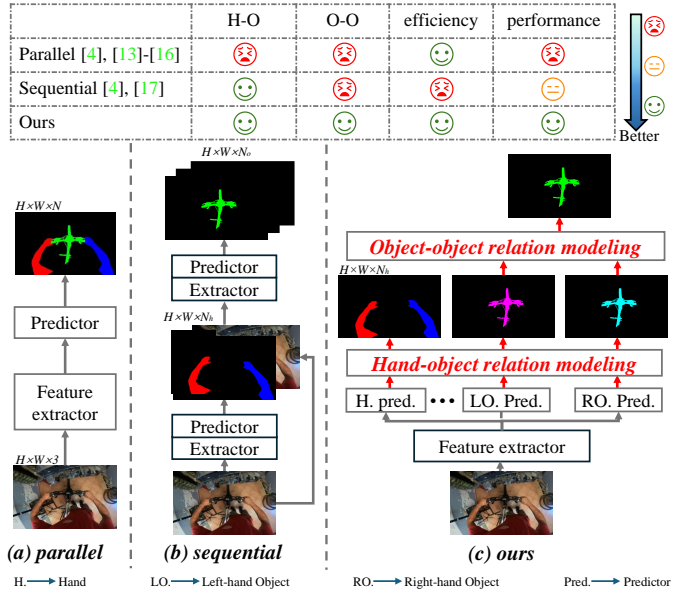


Fig. 1. Structural differences between the previous (a) parallel method, (b) sequential method, and (c) our approach. Compared with previous parallel and sequential methods, the proposed ORMNet can achieve higher segmentation performance with higher efficiency by integrating relationship modeling between “hands and objects (H-O)” as well as “objects and objects (O-O).” The  $N$ ,  $N_h$ , and  $N_o$  mean the number of overall categories, the number of hand categories, and the number of object categories, and  $N = N_h + N_o$ .

(EgoHOS) task, which aims to perform pixel-level segmentation of the hand and the objects that interact with the hand in egocentric images. This novel segmentation task enables a precise response to the query, “*Where are the left and right hands, and what objects are they interacting with?*” which can function as an essential algorithm serving as the foundation for various subsequent applications, such as augmented reality/virtual reality (AR/VR) [5], [6], medical assistant [7], [8], robotics [9], embodied AI [10], [11], and metaverse [12].

The previous approaches for EgoHOS can be categorized into parallel and sequential methods. Specifically, parallel methods [4], [13]–[16] are straightforward, which employ an end-to-end encoder-decoder framework to extract features and predict the mask of all categories simultaneously, as shown in Fig. 1(a). In contrast to parallel methods, sequential approaches [4], [17] employ a step-by-step prediction scheme for the hand and interacting objects, *i.e.*, the input of the latter step to predict the objects’ masks necessitates the previous step’s output for predicting the hand, as depicted in Fig. 1(b).

Although existing methods have demonstrated a satisfied EgoHOS capability, they are accompanied by many drawbacks, as shown in the table in Fig. 1. **First**, similar to conven-

tional encoder-decoder semantic segmentation networks [18], [19], the intuitive parallel approaches [4] regard hands and objects as independent categories and predict segmentation results for them in an end-to-end manner. While this type of technique demonstrates high efficiency, it fails to capture the relationship between “hands and objects” or among different objects, consequently leading to performance deficiencies.

**Second**, in contrast, the sequential methods [4] specially built for the EgoHOS task demonstrate enhanced performance by incorporating the relationships between hands and interacting objects. However, step-wise training and inference elongate the overall time consumption, thereby reducing the method’s efficiency and constraining its feasibility for real-time applications. **Third**, the prediction of diverse interacting objects is required in the EgoHOS task, *i.e.*, left-hand objects (objects interact with the left hand), right-hand objects (objects interact with the right hand), and two-hand objects (objects interact with both hands at the same time). This paper observes the coupling relationship between these three categories of objects, *i.e.*, the two-hand object can be regarded as both a left-hand object and a right-hand object. Therefore, it is easy to predict a two-hand object as the left-hand object when the left interaction is more obvious than the right interaction, and the same applies to the right-hand object. Nevertheless, prevailing methods overlook the ambiguity of such relationships, which introduces confusion during network training.

To improve efficiency and effectiveness simultaneously, this paper proposes a novel end-to-end **Object-centric Relationship Modeling Network** (ORMNet) to model the relationship between “*hands and objects*” as well as “*objects and objects*,” as shown in Fig. 1(c). On the one hand, we propose the Hand-Object Relation (HOR) module to establish the correlation between the features of the hand and interacting objects. The core underlying concept involves leveraging hand features as prior knowledge and employing hand-guided attention to extract more representative object features. On the other hand, we introduce a new Object Relation Decoupling (ORD) strategy to model the relationship among diverse object categories. Drawing from the insights gained from analyzing two-hand objects, this strategy restricts the prediction to left- and right-hand objects exclusively during the training phase. Then, two-hand objects are generated through a simple yet efficient *intersection* operation during inference. This strategy can reduce the confusion of the algorithm about the object categories during learning, enabling the network to concentrate more precisely on the interacting objects. The contributions of this paper are as follows:

- This paper introduces a novel end-to-end ORMNet for the EgoHOS task that achieves state-of-the-art segmentation performance while being highly efficient.
- To take full advantage of the prominence of hand features, the proposed HOR module models the relationship between hands and objects, helping the network extract more comprehensive hand and object features.
- Based on the relation of various object categories, the simple yet powerful ORD strategy is proposed to decouple the two-hand objects during training, reducing

the ambiguity of the network and further separately highlighting the objects contacted with left or right hands.

- The experimental results on two datasets demonstrate that the proposed ORMNet achieves exceptional performance and manifests robust generalization capabilities.

## II. RELATED WORKS

### A. Image Segmentation

Image segmentation is a basic task of computer vision, which aims to divide the image into several non-overlapping regions based on certain principles, such as semantic information. Semantic segmentation [20]–[22], instance segmentation [23]–[25], and panoptic segmentation [26]–[28] are three commonly studied segmentation sub-tasks. Image segmentation methods can be divided into traditional methods, convolution neural network (CNN)-based methods, and transformer-based methods in chronological order. Although traditional methods can perform image segmentation with notable interpretability, further refinement is needed to enhance the quality of the segmentation outcomes. The fully connected neural network (FCN) [19] proposed by Jonathan *et al.* is the cornerstone of CNN segmentation methods. After that, there have been numerous advancements [29] in CNN-based image segmentation methods, such as U-Net [18], Deeplab-series [30], [31], SegNet [32], PSPNet [33], etc.

The development of transformer-based methods for image segmentation is a relatively recent but rapidly evolving field. Dosovitskiy *et al.* introduced the Vision Transformer (ViT) [34] in 2020, proving that the transformer could be applied directly to images by treating the image as a sequence of patches. Following the success of ViT, several transformer-based methods [35] specially designed for image segmentation have been proposed. Zheng *et al.* developed the SETR [36] to adopt ViT as a backbone to extract features to eliminate the reliance on FCN, achieving impressive performance. Similarly, Strudel *et al.* proposed a pure end-to-end Transformer approach - Segmenter [37], which utilized the ViT encoder for capturing global context and a simple point-wise linear decoder to generate precise segmentation masks. Meanwhile, Xie *et al.* presented the Segformer [13] to integrate hierarchical Transformer encoder with lightweight multi-layer perceptron (MLP) decoders, avoiding complex designs in segmentation methods. Unlike previous work, Cheng *et al.* proposed the MaskFormer [38], which abandoned the per-pixel classification formulation and instead predicted a series of binary masks associated with class labels. Following that, Cheng *et al.* introduced the Mask2Former [39], which incorporated masked attention to perform universal (*i.e.*, instance, semantic, and panoptic) segmentation, achieving notable performance. Then, Jain *et al.* proposed OneFormer [14] to perform universal segmentation tasks with transformers and task-guided queries, which achieved state-of-the-art performance in various segmentation benchmarks. Recently, Kirillov *et al.* proposed a new impressive work called Segment Anything (SAM) [40]. They built a foundation model for interactive segmentation by training with over 1 billion masks on 11M images.

Our paper utilizes the Swin transformer [41] to extract the features of the input egocentric image and to up-sample the

features to the input size [15]. Although using more recent methods may improve performance, this is not the main focus of this paper.

### B. Egocentric Hand-object Segmentation

Zhang *et al.* [4] recently introduced a novel task known as Egocentric Hand-object Segmentation (EgoHOS), which combines image segmentation and Human-Object Interaction detection (HOI-det). This task redefines the focus of HOI-det from the entire human body to specific, fine-grained parts, *i.e.*, human hands. Its objective is to segment the left hand, right hand, and the objects that interact with the left and right hands in input RGB egocentric images. Concurrently, Zhang *et al.* [4] introduced the innovative concept of the contact boundary (CB), representing the region where the hands and the objects engage in interaction. This concept explicitly promotes the network focus on the interaction between hands and objects. Furthermore, based on the proposed task and concept, the authors also proposed different types of methods in their work, including parallel methods and sequential methods.

*Parallel method.* A more direct and naive method is to use an encoder and a decoder to segment and predict hands and objects and use different indexes to imply different categories [4], [13]–[16], as shown in Fig. 1(a). Although this parallel method completes the prediction of this task simply and directly, its segmentation accuracy is relatively low and still needs to be improved.

*Sequential method.* Since parallel methods lacked targeted design in learning hand-object interaction, Zhang *et al.* proposed a sequential method [4], as shown in Fig. 1(b). Taking the egocentric image as input, this step-by-step sequential method uses an encoder-decoder first to segment the left and right hands. After that, the segmented left- and right-hand masks are concatenated to the input image to be used to perform the mask prediction of contact boundary and interacting objects. Although the sequential method achieved higher segmentation performance than the parallel method, it lacks efficiency due to the step-by-step process.

In addition, both parallel and sequential methods inadequately explore the relationship between hands and objects and ignore the relationship between objects and objects. Unlike the previous parallel and sequential methods, the proposed ORMNet can achieve end-to-end training and inference with high accuracy due to the relationship modeling between “hands and objects” as well as “objects and objects.”

### C. Attention Mechanism in deep learning

Models using the attention mechanism have exploded in recent years, confirming the effectiveness of the attention mechanism for NLP [42], [43] and computer vision [44], [45] tasks. The primary objective of attention in vision is to mimic the selective function of the human visual cognitive system towards input information, *i.e.*, concentrating on the primary and crucial features of the input visual data. The majority of attention modules utilize distinct methodologies to generate an attention map for feature weighting, consequently adjusting the significance of individual components within the features.

In the early stage, most attention modules are integrated into the CNN-based models. For example, Hu *et al.* proposed the

SENet [46] equipped with channel-wise attention, which used global average pooling to generate the attention weight among channel axial. After that, Woo *et al.* proposed CAM [47] to improve channel attention by aggregating the descriptors from max-pooling and average-pooling. There are many other methods intended to improve channel-wise attention, *e.g.*, SOCA [48], HA [49], *etc.* Unlike channel attention, spatial attention is proposed to generate weights for spatial patches of feature maps. For example, Woo *et al.* proposed SAM [47] to use a convolutional layer to obtain the attention weights.

The development of self-attention and multi-head self-attention (MHSA) mechanisms in transformer-based models has also been widely used in various methods in recent years. Some researchers also make an effort to extend self-attention to cross-attention [50], [51], which allows the model to capture relationships between different modalities of data [52], [53]. The proposed ORMNet utilizes hand-guided cross-attention to model the relationship between the features of hands and objects, allowing more comprehensive feature extraction.

## III. METHODOLOGY

This section introduces the proposed method in detail from top to bottom, including task description (in Sec. III-A), overall architecture (in Sec. III-B), Object Relation Decoupling Strategy (in Sec. III-E), Hand-Object Relation module (in Sec. III-D), and training and inference (in Sec. III-F).

### A. Task Description

The EgoHOS dataset [4] includes the label of the hands, 1<sup>st</sup>-order interacting objects, and 2<sup>nd</sup>-order interacting objects. In this paper, we focus on the segmentation of hands and 1<sup>st</sup>-order interacting objects, *i.e.*, objects that are **directly** contacted by hands. Given an egocentric image  $\mathbf{I}$ , the goal of the EgoHOS task is to predict the masks of the following entities: left hand  $\mathbf{M}_H^L$ , right hand  $\mathbf{M}_H^R$ , left-hand objects  $\mathbf{M}_O^L$  (objects directly interacting with the left hand), right-hand objects  $\mathbf{M}_O^R$  (objects directly interacting with the right hand), and two-hand objects  $\mathbf{M}_O^T$  (objects interacting with both hands simultaneously).

### B. Overall Architecture

The Overall diagram of the proposed ORMNet is shown in Fig. 2. The model consists of an encoder, a bottleneck, and a decoder with multiple branches. The encoder is used to extract distinguishing features of the input egocentric image, the bottleneck is used to enhance the extracted global features, and different branches of the decoder are used to predict the final segmentation masks for diverse categories. Following the previous work [4], ORMNet also contains the contact boundary (CB) decoder branch to predict the mask of the contact boundary. For simplification, we remove the CB decoder branch in Fig. 2.

### C. Encoder and Bottleneck

Taking an egocentric image  $\mathbf{I} \in \mathbb{R}^{H \times W \times 3}$  as input, the first step of ORMNet is to use the image encoder to extract the multi-scale features  $\mathbf{F}_i \in \mathbb{R}^{H_i \times W_i \times C_i}$  by a series of down-sampling by a factor of 2, where  $H_i$ ,  $W_i$ , and  $C_i$  are the height,

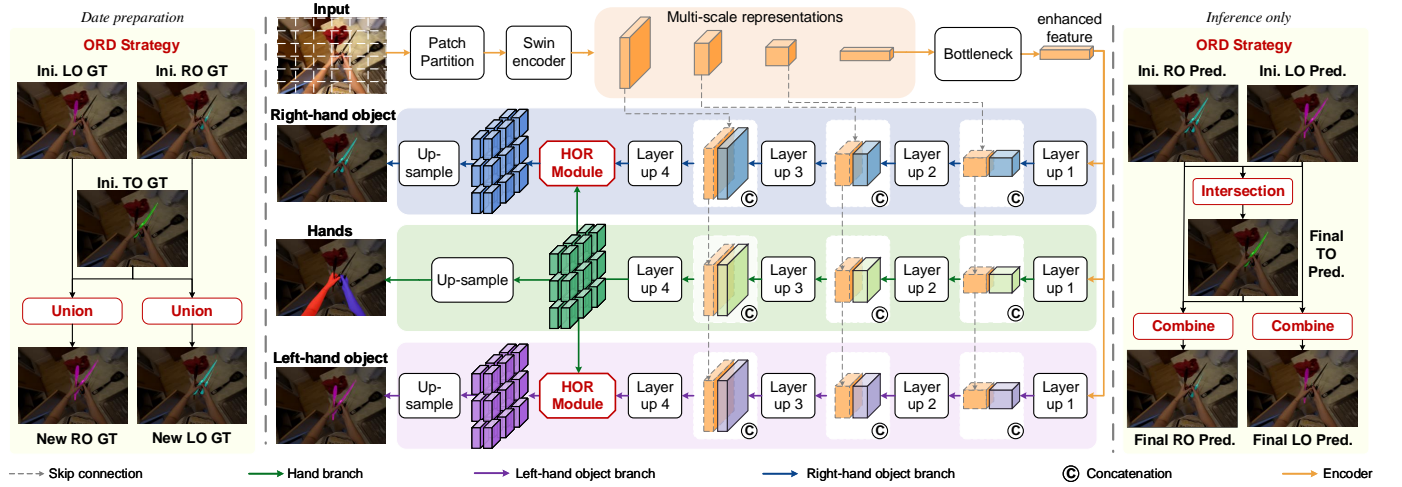


Fig. 2. Overall diagram of the proposed ORMNet, which consists of an encoder, bottleneck, multiple decoder branches, Hand-Object Relation (HOR) module, and Object Relation Decoupling (ORD) strategy. The algorithm is utilized to predict the hands, right-hand objects (RO), left-hand objects (LO), and two-hand objects (TO). The ORD strategy processes the initial (Ini.) ground truth (GT) to generate new supervision during data preparation, and it also processes the predictions (Pred.) of diverse categories of interacting objects during inference.

width, and channel of the  $i^{th}$  stage feature map, respectively. The image encoder used in practice is the Swin Transformer encoder [41]. The extraction process of generating multi-scale features in the encoder can be expressed as follows:

$$\mathbf{F}_{i+1} = f_{enc}^{i+1}(\mathbf{F}_i | W_{enc}^{i+1}), i \in \{0, 1, 2\}, \quad (1)$$

$$\mathbf{F}_0 = f_{enc}^0(\mathbf{I} | W_{enc}^0), \quad (2)$$

where the  $f_{enc}^i(\cdot)$  denotes the encoder stage with the down-sampling for generating the  $i^{th}$  stage feature map, and the  $W_{enc}^i$  represents corresponding parameters.

After generating the multi-scale features, the final feature map with the smallest height and width and the largest channel is sent into the bottleneck to enhance the representation of the encoded feature. Following the work [15], the bottleneck is composed of a patch merging layer and two Swin Transformer blocks, which is denoted as follows:

$$\mathbf{F}_{ehc} = f_{bot}(\mathbf{F}_{last} | W_{bot}), \quad (3)$$

where the  $\mathbf{F}_{last}$  and  $\mathbf{F}_{ehc}$  represent the final encoded feature map and enhanced final feature map, and the  $f_{bot}(\cdot)$  denotes the bottleneck network with the parameter of  $W_{bot}$ . The obtained enhanced memory feature  $\mathbf{F}_{ehc}$  and multi-scale features  $\{\mathbf{F}_i | i = 0, 1, 2\}$  are then passed into separate decoder branches to predict the hands and interacting objects.

#### D. Hand-Object Relation Module

Among the egocentric visual information, the hand information of the HMD wearer is the most prominent and representative. Moreover, the interacted objects can only be identified based on whether they are in contact with the hand rather than appearance and texture cues. Therefore, using hand features to enhance the extraction and expression of object features is beneficial to the EgoHOS task, which has been ignored in previous work. This paper proposes the HOR module to model the correlation between hand features and object features in interaction. Specifically, this module uses representative hand features as priors and guidance and utilizes

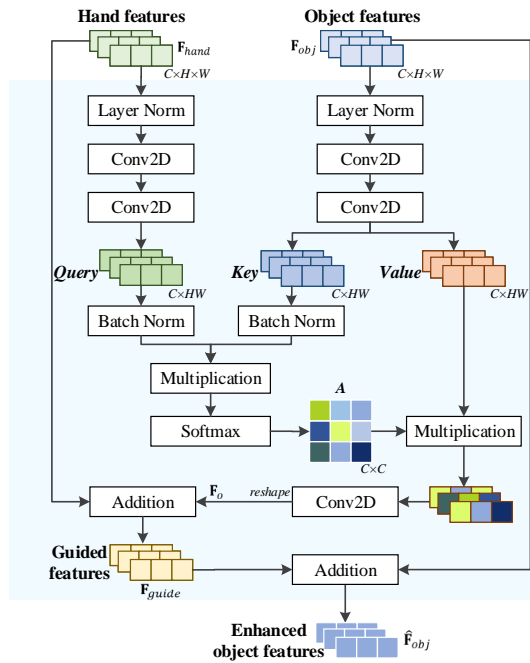


Fig. 3. Detailed architecture of the proposed HOR module. Taking the features of hands and objects as input, this module accomplishes hand-guided attention to model the relationship between the hands and interacting objects, promoting the object feature learning of the network.

the hand-guided attention mechanism to guide the learning of object features, as shown in Fig. 3.

Taking the hand features  $\mathbf{F}_{hand} \in \mathbb{R}^{\hat{C} \times \hat{H} \times \hat{W}}$  and the object features  $\mathbf{F}_{obj} \in \mathbb{R}^{\hat{C} \times \hat{H} \times \hat{W}}$  generated by decoder branches as the input, this module aims to use hand features to enhance the object features to focus more precisely on the interacting region, where  $\hat{C}$ ,  $\hat{H}$ , and  $\hat{W}$  are the channel, height, and width of the feature map. First, two stacked convolution operations are used after the LayerNorm layer to generate the query, key, and value. The query  $Q \in \mathbb{R}^{\hat{C} \times \hat{H} \hat{W}}$  is generated from hand features, and the key  $K \in \mathbb{R}^{\hat{C} \times \hat{H} \hat{W}}$  and value  $V \in \mathbb{R}^{\hat{C} \times \hat{H} \hat{W}}$  are generated from object features, which can be denoted as

follows,

$$Q = f_{conv}(f_{conv}(f_{ln}(\mathbf{F}_{hand}))), \quad (4)$$

$$K, V = f_{conv}(f_{conv}(f_{ln}(\mathbf{F}_{obj}))). \quad (5)$$

After that, the query and key are used to perform the hand-guided attention operation, *i.e.*,

$$\mathbf{A} = \delta(\text{Matmul}(\text{Norm}(Q), \text{Norm}(K^T))), \quad (6)$$

$$\mathbf{F}_o = \text{Conv}(\text{Matmul}(\mathbf{A}, V)), \quad (7)$$

where the  $\mathbf{F}_o$  is the output after convolution, the *Matmul* means the matrix multiplication, and the  $\delta(\cdot)$  represents the softmax function. Then, the input hand features are added to the  $\mathbf{F}_o$  to generate the guided features. Finally, the addition between guided features and original object features is performed to enhance the representation of the object features, which can be described as follows,

$$\mathbf{F}_{guide} = \mathbf{F}_o + \mathbf{F}_{hand}, \quad \hat{\mathbf{F}}_{obj} = \mathbf{F}_{obj} + \mathbf{F}_{guide}, \quad (8)$$

where the  $\hat{\mathbf{F}}_{obj}$  is the output enhanced object features.

#### E. Object Relation Decoupling Strategy

Based on the proposed HOR module, a naive way is to use one decoder branch to predict hands and another decoder branch to predict interacting objects. Then, the HOR module can establish the relation between hands and objects, as shown in Sec. III-D.

However, this paper argues that in this way, the three different types of objects, *i.e.*, left-hand objects, right-hand objects, and two-hand objects, are coupled, which will cause confusion and ambiguity when training the network. In particular, if the network is trained to predict left-hand objects and right-hand objects based on whether they are in contact with the left and right hands, then two-hand objects that are in contact with both hands simultaneously are likely to be confused with either left-hand objects or right-hand objects.

Therefore, different from previous work, our method proposes the ORD strategy to decouple the three kinds of objects according to their physical meanings. Specifically, we consider two-hand objects to be both left-hand and right-hand objects so that two-hand objects can be represented by the intersection of the other two categories. This approach establishes a relationship between two-hand objects and the other two categories that are originally unrelated, enabling the network to concentrate solely on the hand-object interaction without classifying the category.

In practice, the ORD process can be divided into data preparation, training, and inference. First, in the phase of data preparation, we consider the ground truth (GT) of two-hand objects in the dataset as both left-hand objects and right-hand objects, so we generate the new GT of left- and right-hand objects by union operation, as shown in Fig. 2 (left). For example, if the value in the two-hand object GT  $\mathbf{G}_{to}$  at the position  $(i, j)$  is 1, then the value of the left-hand object GT  $\mathbf{G}_{lo}$  and right-hand object GT  $\mathbf{G}_{ro}$  at  $(i, j)$  will be set to 1. The process is shown below,

$$\hat{\mathbf{G}}_{lo} = \mathbf{G}_{lo} \bigcup \mathbf{G}_{to}, \quad \hat{\mathbf{G}}_{ro} = \mathbf{G}_{ro} \bigcup \mathbf{G}_{to}, \quad (9)$$

where the  $\bigcup$  means the union operation, the  $\hat{\mathbf{G}}_{lo}$  and  $\hat{\mathbf{G}}_{ro}$  are the generated GT labels for left-hand objects and right-hand objects.

Then, in the training process, we only use  $\hat{\mathbf{G}}_{lo}$  and  $\hat{\mathbf{G}}_{ro}$  to supervise the two object prediction branches, as shown in Fig. 2, which can be expressed as follows,

$$\hat{\mathbf{M}}_O^L = f_{dec}^{lo}(\mathbf{F}_{ehc}, \mathbf{F}, W_{dec}^{lo}), \quad \mathbf{F} = \{\mathbf{F}_i | i = 0, 1, 2\}, \quad (10)$$

$$\hat{\mathbf{M}}_O^R = f_{dec}^{ro}(\mathbf{F}_{ehc}, \mathbf{F}, W_{dec}^{ro}), \quad \mathbf{F} = \{\mathbf{F}_i | i = 0, 1, 2\}, \quad (11)$$

$$\mathcal{L}_{lo} = l_{ce}(\hat{\mathbf{M}}_O^L, \hat{\mathbf{G}}_{lo}), \quad \mathcal{L}_{ro} = l_{ce}(\hat{\mathbf{M}}_O^R, \hat{\mathbf{G}}_{ro}), \quad (12)$$

where the  $\hat{\mathbf{M}}_O^L$  and  $\hat{\mathbf{M}}_O^R$  are the predicted left-hand objects and right-hand objects. The  $f_{dec}^{lo}(\cdot)$  and  $f_{dec}^{ro}(\cdot)$  represent the decoder branch of left-hand objects and right-hand objects with parameters of  $W_{dec}^{lo}$  and  $W_{dec}^{ro}$ . And the  $\mathcal{L}_{lo}$  and  $\mathcal{L}_{ro}$  denote the loss function of left-hand objects and right-hand objects, which we use the cross entropy  $l_{ce}(\cdot)$  in practice.

In inference, based on the predicted left- and right-hand objects  $\hat{\mathbf{M}}_O^L$  and  $\hat{\mathbf{M}}_O^R$ , the two-hand objects are generated by a simple but effective operation, *i.e.*, intersection, as shown in Fig. 2 (right) and follows,

$$\mathbf{M}_O^T = \hat{\mathbf{M}}_O^L \bigcap \hat{\mathbf{M}}_O^R, \quad (13)$$

$$\mathbf{M}_O^L = \hat{\mathbf{M}}_O^L - \mathbf{M}_O^T, \quad \mathbf{M}_O^R = \hat{\mathbf{M}}_O^R - \mathbf{M}_O^T,$$

where the  $\bigcap$  means the intersection operation, and the  $\mathbf{M}_O^L$  and  $\mathbf{M}_O^R$  are the final left- and right-hand object predictions.

The proposed ORD strategy implicates the physical meaning of the three kinds of objects, especially the meaning of the two-hand objects, *i.e.*, objects that interact with both hands simultaneously. Furthermore, in this way, the network can be trained only to predict the objects that interact with the left-/right-hand rather than focusing on classifying the category of the objects, which achieves decoupling the objects and decreasing the confusion and ambiguity of the algorithm.

#### F. Training and inference

The overall ORMLNet is trained by the weighted cross-entropy loss function between predictions and GTs of hands, left-hand objects, right-hand objects, and contact boundaries. The overall loss function  $\mathcal{L}$  can be computed by,

$$\mathcal{L} = \alpha(l_{ce}(\mathbf{M}_O^L, \hat{\mathbf{G}}_{lo}) + l_{ce}(\mathbf{M}_O^R, \hat{\mathbf{G}}_{ro}),) + \gamma l_{ce}(\mathbf{M}_H, \mathbf{G}_h) + \lambda l_{ce}(\mathbf{M}_{CB}, \mathbf{G}_{cb}), \quad (14)$$

where the  $l_{ce}(x, y)$  means the cross entropy loss between  $x$  and  $y$ , the  $\mathbf{M}_{CB}$  and  $\mathbf{G}_{cb}$  are the prediction and GT of the contact boundary, respectively. The GT of the contact boundary is generated by the GT of the hands and interacting objects automatically, which is the overlapping region of the dilated hand and object masks [4].

For inference, as stated in Sec. III-E, the network predicts the masks of hands, left-hand objects, and right-hand objects, and then the mask of the two-hand objects can be obtained by the proposed ORD strategy.

TABLE I

COMPARISON RESULTS ON THE EGOHOS IN-DOMAIN TEST SET MEASURED BY IOU/ACC AND MIoU/mACC. THE “ $\prime$ ” MEANS THE METHOD WITH DATA AUGMENTATION, THE “ $\diamond$ ” MEANS THE METHOD INTRODUCED CONTACT BOUNDARY, AND THE “ $\flat$ ” MEANS THE METHOD WITH DATA AUGMENTATION AND CONTACT BOUNDARY.

Method	Type	Backbone	Left hand	Right hand	Left-hand objects	Right-hand objects	Two-hand objects	Overall
			IoU(%)   Acc(%)	mIoU(%)   mAcc(%)				
Segformer [13]	parallel	MiT [13]	62.49   75.47	64.77   78.13	4.03   4.57	3.01   3.17	5.13   5.57	27.89   33.38
SCTNet [54]	parallel	SCTNet [54]	81.94   90.25	82.12   89.92	17.77   24.49	16.60   20.79	21.74   29.08	44.03   50.91
Para. $\prime$ [4]	parallel	Swin-B	77.57   -	81.06   -	54.83   -	38.48   -	39.14   -	58.22   -
Segformer [13]	parallel	Swin-B	65.36   78.20	66.26   79.21	11.63   15.45	8.07   9.24	12.48   15.97	32.76   39.61
Para. [4]	parallel	Swin-B	69.08   75.57	73.50   75.93	48.67   39.50	36.21   39.33	37.46   42.58	52.98   54.58
Segmenter [37]	parallel	Swin-B	82.20   89.87	83.28   91.92	46.22   62.69	34.79   45.59	51.10   62.78	59.52   70.57
UperNet [16]	parallel	Swin-B	89.88   89.86	91.39   91.32	36.22   37.24	40.55   42.26	45.54   49.27	60.71   61.99
Segmenter [37]	parallel	ViT [34]	88.47   95.66	89.29   95.08	49.87   61.14	40.60   57.07	46.96   60.81	63.04   73.95
MaskFormer [38]	parallel	Swin-B	90.45   95.90	91.95   96.41	43.51   67.08	41.04   52.91	54.65   64.86	64.32   75.43
Mask2Former [39]	parallel	Swin-B	90.74   96.01	92.25   96.20	44.22   53.97	46.05   58.10	51.13   60.48	64.88   72.95
Seq. [4]	sequential	Swin-B	73.17   -	80.56   -	54.83   -	38.48   -	39.14   -	57.24   -
Seq. $\diamond$ [4]	sequential	Swin-B	77.25   -	81.17   -	59.05   -	40.85   -	49.94   -	61.65   -
Seq. $\prime$ [4]	sequential	Swin-B	87.70   -	88.79   -	58.32   -	40.18   -	46.24   -	64.25   -
Seq. $\flat$ [4]	sequential	Swin-B	87.70   95.77	88.79   91.29	62.20   66.67	44.40   59.85	52.77   62.21	67.17   75.16
<b>ORMNet</b>	parallel	Swin-B	<b>92.34   96.64</b>	<b>93.64   96.81</b>	60.07   <b>71.79</b>	<b>56.69   68.71</b>	<b>54.73   65.85</b>	<b>71.49   79.96</b>

#### IV. EXPERIMENTS

This section first introduces the datasets and metrics we used to validate the EgoHOS performance. Second, we compare the proposed ORMNet with state-of-the-art methods in the EgoHOS task. Then, we ablate the import design strategy and elements of ORMNet.

##### A. Datasets and Metrics

**EgoHOS.** The EgoHOS [4] dataset consists of 11,743 egocentric images containing per-pixel segmentation labels of hands and interacting objects, gathered from Ego4D [55], EPICKITCHEN [56], THU-READ [57], and their own collected egocentric videos. Among them, 8,993 images are used for training, 1,124 images are for validation, 1,126 images are used for in-domain testing, and 500 images are used for out-of-domain testing.

**mini-HOI4D.** HOI4D [58] is a large-scale egocentric image and video dataset with rich annotations for category-level hand-object interaction. Frame-wise annotations for action segmentation, motion segmentation, panoptic segmentation, 3D hand pose, and category-level object pose are also provided, together with reconstructed object meshes and scene point cloud. In order to test the generalization of the proposed ORMNet, this paper further tests the proposed model with other comparative methods on the HOI4D dataset. Since the HOI4D dataset includes the masks of the hand and all objects that have interacted with the hand in a video, we first extract the masks of the objects currently interacting with the hand and delete other objects’ masks. Then, we map the label of the interacting objects to the left-hand objects, right-hand objects, and two-hand objects. Finally, we sampled a total of 1,095 egocentric images, forming a new dataset mini-HOI4D, to test the generalization of the algorithms on the EgoHOS task.

Following most related works, this paper uses the most common and widely used metrics in the segmentation task to evaluate the performance, *i.e.*, we use Intersection-over-Union (IoU) and pixel Accuracy (Acc) for each category. Mean IoU (mIoU) and mean accuracy (mAcc) are also employed to indicate the overall performance.

##### B. Implementation Details

The experiments were conducted on 4 NVIDIA RTX 6000 Ada GPUs. The batch size was set to 12. Data preparation included cropping the image to (448, 448) and normalization with the mean of [106.011, 95.400, 87.429], and the standard deviation was set to [64.357, 60.889, 61.419]. The patch size of the Swin transformer encoder was set to 4, and the window size was set to 12. The AdamW optimizer was used in the experiment, the learning rate was set to 1e-5, and the weight decay was set to 0.01.

##### C. Quantitative Results

1) *Comparison results on EgoHOS in-domain test set.* Table I presents the comparison results of our proposed ORMNet against state-of-the-art methods on the EgoHOS in-domain test set. In addition to the parallel (Para.-series) and sequential methods (Seq.-series) proposed in Zhang’s work [4] introduced in detail in Sec. II-B, we also select some of the latest transformer-based models with different backbones as parallel methods to compare the effectiveness of the model, *e.g.*, Segformer [13], Segmenter [37], MaskFormer [38], and Mask2former [39], and SCTNet [54]. All these methods are trained on the EgoHOS train set and tested on the in-domain test set using the same parameter setting as the proposed ORMNet. In general, the proposed ORMNet far outperforms all previous methods in most categories on both metrics. Specifically, compared with the previous best parallel method

TABLE II  
COMPARISON RESULTS ON THE EGOHOS OUT-OF-DOMAIN TEST SET.

Method	Type	Backbone	Left hand		Right hand		Left-hand objects		Right-hand objects		Two-hand objects		Overall	
			IoU(%)	Acc(%)	IoU(%)	Acc(%)	IoU(%)	Acc(%)	IoU(%)	Acc(%)	IoU(%)	Acc(%)	mIoU(%)	mAcc(%)
Segformer [13]	parallel	MiT [13]	71.97	87.33	71.44	81.75	7.60	8.34	5.00	5.65	4.91	5.95	32.18	37.80
Segformer [13]	parallel	Swin-B	74.01	86.80	70.84	79.44	15.61	21.77	7.32	9.56	8.29	11.67	35.21	41.85
SCTNet [54]	parallel	SCTNet [54]	87.12	94.62	86.29	90.92	31.18	49.14	19.70	27.47	13.32	17.12	47.52	55.85
UperNet [16]	parallel	Swin-B	93.17	96.89	93.96	96.00	42.53	64.83	28.88	54.59	24.35	27.83	56.58	68.03
Segmenter [37]	parallel	Swin-B	83.13	91.22	84.85	92.56	57.97	72.44	38.59	52.75	44.98	52.88	61.90	72.37
Maskformer [38]	parallel	Swin-B	92.69	95.58	94.02	96.10	51.81	70.53	39.84	60.49	39.43	46.52	63.56	73.84
Mask2former [39]	parallel	Swin-B	91.46	97.05	93.04	96.38	53.41	64.39	44.90	64.18	35.61	39.78	63.68	72.36
Segmenter [37]	parallel	ViT [34]	89.40	95.02	90.58	94.86	52.73	75.75	43.88	56.34	42.33	51.08	63.78	74.61
Seq. <sup>b</sup> [4]	sequential	Swin-B	81.77	87.83	78.82	85.98	46.93	57.17	26.40	43.85	42.38	54.76	55.26	65.92
<b>ORMNet</b>	parallel	Swin-B	<b>94.47</b>	<b>97.09</b>	<b>94.41</b>	<b>96.69</b>	51.56	72.30	36.80	60.90	41.84	46.28	<b>63.82</b>	<b>74.65</b>

TABLE III

COMPARISON RESULTS ON THE MINI-HOI4D TEST SET. NOTE: THE LEFT-HAND OBJECTS ARE NOT CONSIDERED TO COMPARE DUE TO FEW SAMPLES.

Method	Type	Backbone	Left hand		Right hand		Right-hand objects		Two-hand objects		Overall	
			IoU(%)	Acc(%)	IoU(%)	Acc(%)	IoU(%)	Acc(%)	IoU(%)	Acc(%)	mIoU(%)	mAcc(%)
Segformer [13]	parallel	Swin-B	27.73	87.97	53.27	66.91	8.43	9.72	9.30	13.40	24.68	44.50
Segformer [13]	parallel	MiT [13]	30.16	92.13	56.44	72.42	5.17	5.52	12.02	13.41	25.95	45.87
SCTNet [54]	parallel	SCTNet [54]	35.83	95.25	66.29	71.27	17.72	22.68	20.98	29.98	35.21	54.80
Segmenter [37]	parallel	Swin-B	70.31	89.02	73.78	89.23	21.82	43.75	44.98	56.97	52.72	69.74
UperNet [16]	parallel	Swin-B	54.82	97.71	84.43	86.04	20.34	25.77	29.34	36.58	47.23	61.53
MaskFormer [38]	parallel	Swin-B	58.50	96.63	83.66	87.83	35.28	44.81	56.91	73.47	58.59	75.69
Segmenter [37]	parallel	ViT [34]	<b>74.70</b>	94.03	85.58	92.34	22.38	44.42	58.67	73.99	60.33	76.20
Mask2Former [39]	parallel	Swin-B	70.13	97.48	88.57	89.38	32.37	45.22	55.72	<b>74.17</b>	61.70	76.56
Seq. <sup>b</sup> [4]	sequential	Swin-B	8.74	40.90	34.60	38.05	23.88	28.99	53.96	61.67	30.30	42.40
<b>ORMNet</b>	parallel	Swin-B	70.39	<b>97.79</b>	<b>89.76</b>	<b>93.09</b>	27.56	<b>49.35</b>	<b>60.08</b>	68.01	<b>61.95</b>	<b>77.06</b>

in the 8<sup>th</sup> row, Mask2Former, our method has demonstrated pronounced advancements across various categories and exhibited particularly notable enhancements in object segmentation. For example, our method showcases substantial enhancements of 15.85%, 10.64%, and 3.6% on left-, right-, and two-hand objects, respectively. Furthermore, compared with the results of the previous best sequential methods Seq<sup>b</sup>, our ORMNet improves IoU by more than 4% on both the left and right hands. The most substantial enhancement is observed in the right-hand objects, surpassing 12%. Finally, compared with the previous best method, our proposed method attains a commendable advancement of 4.33% and 4.55% in mIoU and mAcc, respectively. This is because we propose an ORD strategy to decouple the relationship between object categories, which reduces the burden of network learning. Furthermore, we propose the HOR module to strengthen the correlation between hand features and object features, significantly improving the segmentation accuracy of hands and objects.

2) *Comparison results on EgoHOS out-of-domain test set.* In order to test the generalization performance of different models, the EgoHOS dataset provides 500 out-of-domain images, which are captured from YouTube and annotated

manually. Table II illustrates the comparison results of our method with the previous methods on the EgoHOS out-of-domain test set measured by IoU and Acc. Please note that some of the results in the table are from direct inference using the officially released best model (if available), and other results are from direct inference on the best model trained on our own. It can be observed that the results of our proposed ORMNet on the two metrics of most categories have obtained competitive generalization performance. Among them, the IoU of the left and right hand exceed 94%, and the Acc. of these two categories exceed 96%. The segmentation results on various object categories also achieve balanced performance. Finally, our ORMNet achieves state-of-the-art performance in overall mIoU and mAcc metrics and demonstrates excellent generalization performance on the out-of-domain test set.

3) *Comparison results on mini-HOI4D dataset.* In addition to the evaluation on the EgoHOS out-of-domain test set, we also assess the model's generalization capabilities using a completely different mini-HOI4D dataset. It should be noted that due to the limited samples of left-hand objects in the original HOI4D [58] dataset, the generated mini-HOI4D dataset does not include samples of left-hand objects. Consequently, no

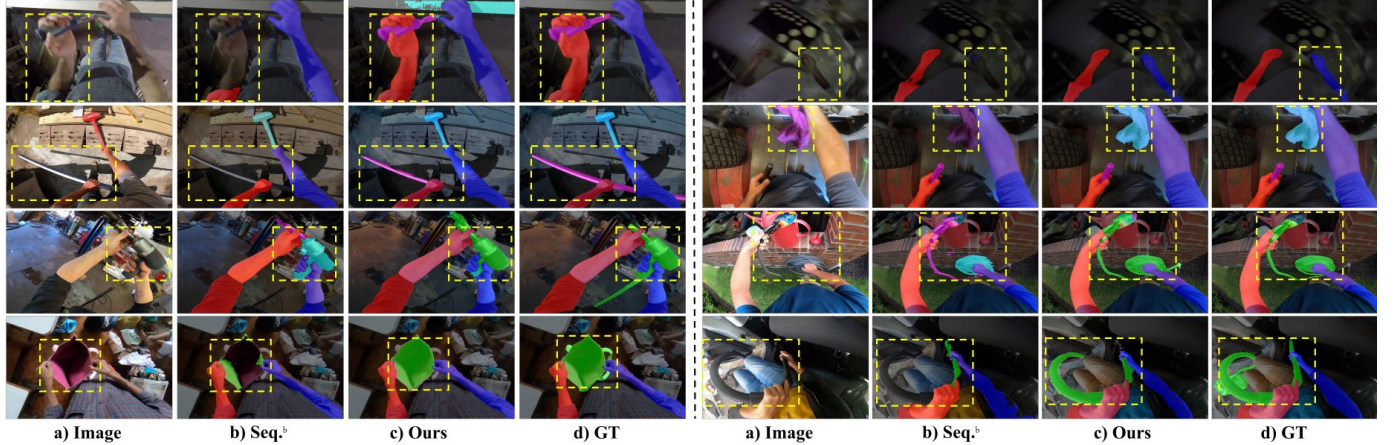


Fig. 4. Visualization results of the ORMNet compared with the sequential method Seq.<sup>b</sup> on the EgoHOS in-domain test set. The main improvements are highlighted in the dashed yellow box. Red: left hand, dark blue: right hand, pink: left-hand objects, green: two-hand objects, and light blue: right-hand objects.

TABLE IV

ABLATION RESULTS ON THE EGOHOS IN-DOMAIN TEST SET UNDER THE SAME SETTING MEASURED BY IOU AND mIoU. LH: LEFT HAND, RH: RIGHT HAND, LO: LEFT-HAND OBJECT, RO: RIGHT-HAND OBJECT, TO: TWO-HAND OBJECT.

Method	Lh (%)	Rh (%)	Lo (%)	Ro (%)	To (%)	mIoU (%)
Basic	90.47	91.02	44.11	45.57	51.08	64.45
Basic+ORD	<b>93.14</b>	<b>93.73</b>	<b>60.86</b>	54.58	49.69	70.40
Basic+HOR	92.76	93.36	44.15	53.68	51.85	67.16
Basic+ORD+HOR	92.34	93.64	60.07	<b>56.69</b>	<b>54.73</b>	<b>71.49</b>

TABLE V

THE EXPERIMENTAL RESULTS USING DIFFERENT HYPER-PARAMETERS.  $\alpha$ ,  $\gamma$ , AND  $\lambda$  ARE THE WEIGHTS OF OBJECTS, HANDS, AND CB LOSSES. LH: LEFT HAND, RH: RIGHT HAND, LO: LEFT-HAND OBJECT, RO: RIGHT-HAND OBJECT, TO: TWO-HAND OBJECT.

$\alpha$	$\gamma$	$\lambda$	Lh (%)	Rh (%)	Lo (%)	Ro (%)	To (%)	mIoU (%)
1.0	1.0	1.0	90.66	91.80	57.38	56.20	52.12	69.63
1.0	0.5	0.5	89.74	90.56	57.8	55.46	51.08	68.93
0.5	0.5	1.0	90.22	91.10	57.78	55.59	50.81	69.10
0.5	1.0	0.5	<b>92.34</b>	<b>93.64</b>	<b>60.07</b>	<b>56.69</b>	<b>54.73</b>	<b>71.49</b>

testing is performed on left-hand objects.

The comparison results on the mini-HOI4D data set are shown in Table III. Similarly to the EgoHOS out-of-domain test set, the results on the mini-HOI4D dataset are directly inferred by utilizing trained and saved checkpoints without further training procedures. Overall, our proposed ORMNet outperforms all the previous parallel and sequential methods concerning mIoU and mAcc. Our method excels notably in hand segmentation, *i.e.*, 1.57% and 3.71% improvements on IoU and Acc for the right hand compared with the 8<sup>th</sup> row. Our method also competes well in interacting object segmentation, yielding commendable outcomes. Therefore, it can be deduced from the results of the EgoHOS out-of-domain and mini-HOI4D test sets that our proposed ORMNet exhibits superior generalization capabilities in contrast to the comparative methods.

4) *Ablation study.* In order to verify the effectiveness of the proposed method alongside its corresponding sub-module and strategy, we conduct the ablation study in this section. The experimental results are shown in Table IV. The basic model uses Swin-B as the encoder and uses three decoder branches

to predict hands, contact boundaries, and objects. This basic model is a naive solution for the EgoHOS task and does not model any relationships between hands and interacting objects, so its results are relatively poor. The 2<sup>nd</sup> and 3<sup>rd</sup> rows of the table show the results after adding the ORD strategy and HOR module independently, which proves that adding them to the basic model is beneficial. The last row is the result after integrating the ORD strategy and the HOR module. By explicitly modeling both the hand-object relationship and the object-object relationship, the segmentation accuracy achieves its peak performance. Generally speaking, although the effect improvement brought by the ORD strategy is higher than that of the HOR module, using these two modules and strategies simultaneously can further improve the segmentation performance, which verifies the effectiveness of our proposed method and sub-methods.

5) *Hyper-parameter experiments.* While identifying the optimal hyper-parameters is not the primary focus of this paper, this section still conducts experiments on the configurations of different hyper-parameters. The experimental results are shown in Table V. We assign the value of  $\alpha$ ,  $\gamma$ , and  $\lambda$  based on the relative significance of the interacting objects, hands, and contact boundaries. In the 1<sup>st</sup> row, all categories are considered equal importance, while in subsequent experiments (*i.e.*, 2<sup>nd</sup>, 3<sup>rd</sup> and 4<sup>th</sup>), we regard the objects, CBs, and hands as the most crucial, respectively. The results lead to the inference that amplifying the importance of hands can yield enhancements in the method's performance, which can be explained intuitively because the proposed HOR module leverages hands as prior knowledge for feature enhancement.

#### D. Qualitative Results

1) *Results on EgoHOS in-domain test set.* This section shows the visual experimental results on the EgoHOS in-domain test set, as shown in Fig. 4. We choose the previous best sequential method Seq.<sup>b</sup> as the comparative method, which is specially designed for the EgoHOS task. We can observe that our method has better performance in segmenting hands, as shown in the results of the 1<sup>st</sup> row. Moreover, since our method proposes an ORD strategy to model the

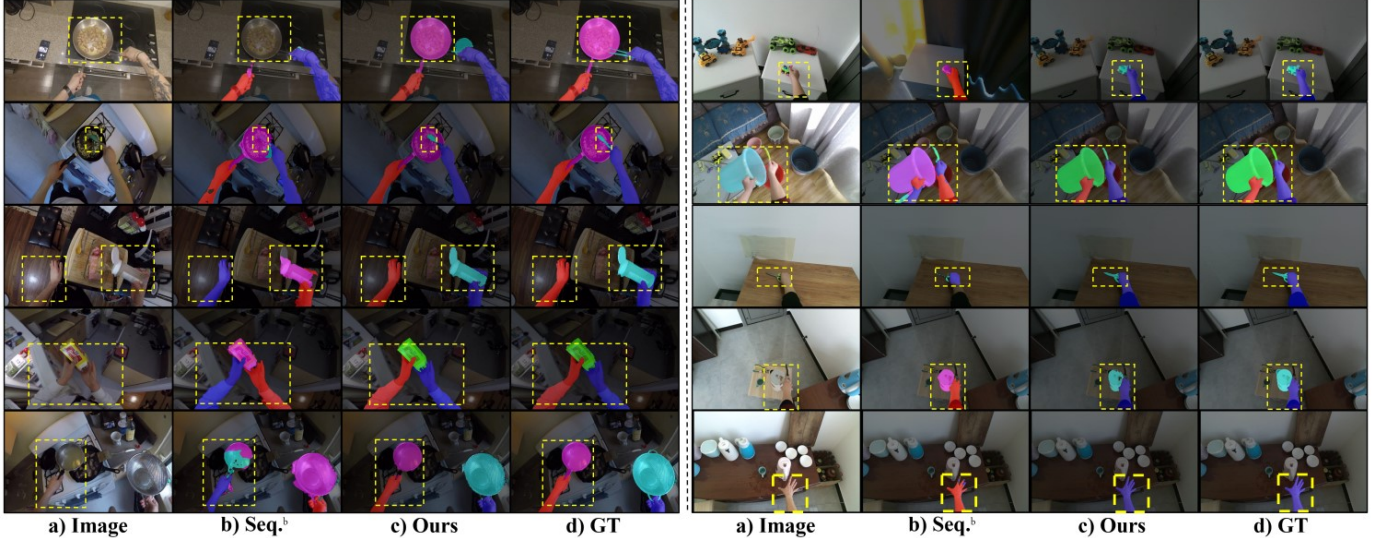


Fig. 5. Visualization results of the ORMNet compared with the sequential method on the EgoHOS out-of-domain test set (left) and mini-HOI4D dataset (right). Red: left hand, dark blue: right hand, pink: left-hand objects, light blue: right-hand objects, and green: two-hand objects.

relationship between diverse objects and reduces the ambiguity of different types of objects, ORMNet also has better consistency and accuracy when segmenting interacting objects, as shown in the results of the 2<sup>nd</sup> row. Furthermore, although our method does not predict two-hand objects through the learnable network, it has higher prediction accuracy and effect, which is shown in the 3<sup>rd</sup> and 4<sup>th</sup> rows. In the results of the comparative method, the two-hand objects or part of them may be segmented into left- and right-hand objects. However, our method only focuses on the objects that the hands interact with during the learning process using the ORD strategy rather than concentrating on “whether the object interacts with the left and right hands at the same time,” thereby enhancing the segmentation consistency and accuracy.

2) *Results on EgoHOS out-of-domain test set.* We directly used the saved checkpoint to conduct experiments on the EgoHOS out-of-domain test set and compared it with the Seq<sup>b</sup> method. The visualized experimental results are shown in Fig. 5 (left). According to the visualization results, our ORMNet has stronger generalization than the compared sequential model. Specifically, our method can segment and identify left and right hands accurately, as shown in the 3<sup>rd</sup> to the last rows of results. Furthermore, our method can precisely segment and recognize different kinds of objects, ensuring consistent segmentation of interactive objects.

3) *Results on mini-HOI4D dataset.* The experiments on the mini-HOI4D dataset are also conducted directly using the saved checkpoints. The experimental results are shown in Fig. 5 (right). It can be observed from the experimental results that the contrasting sequential method easily confuses the left and right hands, such as 1<sup>st</sup>, 2<sup>nd</sup>, 4<sup>th</sup>, and 5<sup>th</sup> rows of the results. In contrast, our method exhibits robust generalization capabilities coupled with outstanding segmentation performance. In addition, although some tiny parts are not considered, such as the handle of the bucket in the third row, our method also significantly excels in segmenting two-hand objects.

## V. CONCLUSION

This paper introduces an end-to-end high-performance Object-centric Relationship Modeling Network to effectively handle the egocentric hand-object segmentation task. First, the HOR module is proposed to facilitate the modeling of hand-object interactions through hand-guided cross-attention, enhancing the network’s adaptability to learn precise representations. Second, this paper designs the ORD strategy to decouple the two-hand objects, thereby reducing the network’s confusion about object segmentation. Experimental results demonstrate that the proposed ORMNet exhibits SOTA segmentation efficacy and robust generalization capabilities across varied datasets.

## VI. ACKNOWLEDGEMENTS

The research work was conducted in the JC STEM Lab of Machine Learning and Computer Vision funded by The Hong Kong Jockey Club Charities Trust.

## REFERENCES

- [1] E. Santos and V. Castillo, “Apple Vision Pro: Comments in Healthcare,” *CoRR*, vol. abs/2401.08685, 2024.
- [2] Y. Zhang, X. Hu, K. Kiyokawa, and X. Yang, “Add-on Occlusion: Building an Occlusion-capable Optical See-through Head-mounted Display with HoloLens 1,” in *Proc. VRW*, 2023, pp. 1003–1004.
- [3] Z. Li, L. Cao, H. Wang, and L. Xu, “End-to-End Instance-Level Human Parsing by Segmenting Persons,” *T-MM*, vol. 26, pp. 41–50, 2024.
- [4] L. Zhang, S. Zhou, S. Stent, and J. Shi, “Fine-Grained Egocentric Hand-Object Segmentation: Dataset, Model, and Applications,” in *Proc. ECCV*, vol. 13689, 2022, pp. 127–145.
- [5] Y. Lin, Y. Lan, and S. Wang, “A Method for Evaluating the Learning Concentration in Head-mounted Virtual Reality Interaction,” *VR*, vol. 27, no. 2, pp. 863–885, 2023.
- [6] R. Shi, Y. Wei, X. Qin, P. Hui, and H. Liang, “Exploring Gaze-assisted and Hand-based Region Selection in Augmented Reality,” *PACM HCI*, vol. 7, no. ETRA, pp. 1–19, 2023.
- [7] C. Li, C. Wong, S. Zhang, N. Usuyama, H. Liu, J. Yang, T. Naumann, H. Poon, and J. Gao, “LLAVA-Med: Training a Large Language-and-Vision Assistant for Biomedicine in One Day,” in *Proc. NeurIPS*, 2023.
- [8] R. Azad, R. Arimond, E. K. Aghdam, A. Kazerouni, and D. Merhof, “DAE-Former: Dual Attention-Guided Efficient Transformer for Medical Image Segmentation,” in *Proc. Predictive Intelligence in Medicine*, vol. 14277, 2023, pp. 83–95.

[9] Z. Li, I. Reyes, and H. Alemzadeh, "Robotic Scene Segmentation with Memory Network for Runtime Surgical Context Inference," in *Proc. IROS*, 2023, pp. 6601–6607.

[10] Y. Huang, G. Chen, J. Xu, M. Zhang, L. Yang, B. Pei, H. Zhang, L. Dong, Y. Wang, L. Wang, and Y. Qiao, "EgoExoLearn: A Dataset for Bridging Asynchronous Ego- and Exo-centric View of Procedural Activities in Real World," *CoRR*, vol. abs/2403.16182, 2024.

[11] K. Grauman, A. Westbury, L. Torresani, K. Kitani, J. Malik, T. Afouras, K. Ashutosh, V. Baiyya, S. Bansal, and et al., "Ego-Exo4D: Understanding Skilled Human Activity from First- and Third-Person Perspectives," *CoRR*, vol. abs/2311.18259, 2023.

[12] K. Lam, L. Yang, A. Alhilal, L. Lee, G. Tyson, and P. Hui, "Human-Avatar Interaction in Metaverse: Framework for Full-Body Interaction," in *Proc. ACMMM*, 2022, pp. 10:1–10:7.

[13] E. Xie, W. Wang, Z. Yu, A. Anandkumar, J. M. Álvarez, and P. Luo, "SegFormer: Simple and Efficient Design for Semantic Segmentation with Transformers," in *Proc. NeurIPS*, 2021, pp. 12 077–12 090.

[14] J. Jain, J. Li, M. Chiu, A. Hassani, N. Orlov, and H. Shi, "OneFormer: One Transformer to Rule Universal Image Segmentation," in *Proc. CVPR*, 2023, pp. 2989–2998.

[15] H. Cao, Y. Wang, J. Chen, D. Jiang, X. Zhang, Q. Tian, and M. Wang, "Swin-Unet: Unet-Like Pure Transformer for Medical Image Segmentation," in *Proc. ECCV*, vol. 13803, 2022, pp. 205–218.

[16] T. Xiao, Y. Liu, B. Zhou, Y. Jiang, and J. Sun, "Unified Perceptual Parsing for Scene Understanding," in *Proc. ECCV*, vol. 11209, 2018, pp. 432–448.

[17] M. Zhang, K. Xie, Y. Zhang, C. Wen, and J. He, "Fine Segmentation on Faces With Masks Based on a Multistep Iterative Segmentation Algorithm," *IEEE Access*, vol. 10, pp. 75 742–75 753, 2022.

[18] O. Ronneberger, P. Fischer, and T. Brox, "U-Net: Convolutional Networks for Biomedical Image Segmentation," in *Proc. MICCAI*, vol. 9351, 2015, pp. 234–241.

[19] J. Long, E. Shelhamer, and T. Darrell, "Fully Convolutional Networks for Semantic Segmentation," in *Proc. CVPR*, 2015, pp. 3431–3440.

[20] J. Zhang, R. Liu, H. Shi, K. Yang, S. Reiß, K. Peng, H. Fu, K. Wang, and R. Stiefelhagen, "Delivering Arbitrary-Modal Semantic Segmentation," in *Proc. CVPR*, 2023, pp. 1136–1147.

[21] Aakanksha and A. N. Rajagopalan, "Improving Robustness of Semantic Segmentation to Motion-Blur Using Class-Centric Augmentation," in *Proc. CVPR*, 2023, pp. 10 470–10 479.

[22] T. Chen, Y. Yao, X. Huang, Z. Li, L. Nie, and J. Tang, "Spatial Structure Constraints for Weakly Supervised Semantic Segmentation," *T-IP*, vol. 33, pp. 1136–1148, 2024.

[23] L. Ke, Y. Tai, and C. Tang, "Occlusion-Aware Instance Segmentation Via BiLayer Network Architectures," *T-PAMI*, vol. 45, no. 8, pp. 10 197–10 211, 2023.

[24] Z. Tian, B. Zhang, H. Chen, and C. Shen, "Instance and Panoptic Segmentation Using Conditional Convolutions," *T-PAMI*, vol. 45, no. 1, pp. 669–680, 2023.

[25] Y. Sun, L. Su, S. Yuan, and H. Meng, "DANet: Dual-Branch Activation Network for Small Object Instance Segmentation of Ship Images," *T-CSVT*, vol. 33, no. 11, pp. 6708–6720, 2023.

[26] S. Saha, L. Hoyer, A. Obukhov, D. Dai, and L. V. Gool, "EDAPS: Enhanced Domain-Adaptive Panoptic Segmentation," in *Proc. ICCV*, 2023, pp. 19 177–19 188.

[27] T. Chen, L. Li, S. Saxena, G. E. Hinton, and D. J. Fleet, "A Generalist Framework for Panoptic Segmentation of Images and Videos," in *Proc. ICCV*, 2023, pp. 909–919.

[28] Q. Chen, A. Cheng, X. He, P. Wang, and J. Cheng, "SpatialFlow: Bridging All Tasks for Panoptic Segmentation," *T-CSVT*, vol. 31, no. 6, pp. 2288–2300, 2021.

[29] Z. Huang, X. Wang, L. Huang, C. Huang, Y. Wei, and W. Liu, "CCNet: Criss-Cross Attention for Semantic Segmentation," in *Proc. ICCV*, 2019, pp. 603–612.

[30] L. Chen, G. Papandreou, I. Kokkinos, K. Murphy, and A. L. Yuille, "DeepLab: Semantic Image Segmentation with Deep Convolutional Nets, Atrous Convolution, and Fully Connected CRFs," *CoRR*, vol. abs/1606.00915, 2016.

[31] Q. Yu, H. Wang, D. Kim, S. Qiao, M. D. Collins, Y. Zhu, H. Adam, A. L. Yuille, and L. Chen, "CMT-DeepLab: Clustering Mask Transformers for Panoptic Segmentation," in *Proc. CVPR*, 2022, pp. 2550–2560.

[32] V. Badrinarayanan, A. Kendall, and R. Cipolla, "SegNet: A Deep Convolutional Encoder-Decoder Architecture for Image Segmentation," *T-PAMI*, vol. 39, no. 12, pp. 2481–2495, 2017.

[33] H. Zhao, J. Shi, X. Qi, X. Wang, and J. Jia, "Pyramid Scene Parsing Network," in *Proc. CVPR*, 2017, pp. 6230–6239.

[34] A. Dosovitskiy, L. Beyer, A. Kolesnikov, D. Weissenborn, X. Zhai, T. Unterthiner, M. Dehghani, M. Minderer, G. Heigold, S. Gelly, J. Uszkoreit, and N. Houlsby, "An Image is Worth 16x16 Words: Transformers for Image Recognition at Scale," in *Proc. ICLR*, 2021.

[35] J. Jain, A. Singh, N. Orlov, Z. Huang, J. Li, S. Walton, and H. Shi, "Se-Mask: Semantically Masked Transformers for Semantic Segmentation," in *Proc. ICCV*, 2023, pp. 752–761.

[36] S. Zheng, J. Lu, H. Zhao, X. Zhu, Z. Luo, Y. Wang, Y. Fu, J. Feng, T. Xiang, P. H. S. Torr, and L. Zhang, "Rethinking Semantic Segmentation From a Sequence-to-Sequence Perspective With Transformers," in *Proc. CVPR*, 2021, pp. 6881–6890.

[37] R. Strudel, R. G. Pinel, I. Laptev, and C. Schmid, "Segmenter: Transformer for Semantic Segmentation," in *Proc. ICCV*, 2021, pp. 7242–7252.

[38] B. Cheng, A. G. Schwing, and A. Kirillov, "Per-Pixel Classification is Not All You Need for Semantic Segmentation," in *Proc. NeurIPS*, 2021, pp. 17 864–17 875.

[39] B. Cheng, I. Misra, A. G. Schwing, A. Kirillov, and R. Girdhar, "Masked-attention Mask Transformer for Universal Image Segmentation," in *Proc. CVPR*, 2022, pp. 1280–1289.

[40] A. Kirillov, E. Mintun, N. Ravi, H. Mao, C. Rolland, L. Gustafson, T. Xiao, S. Whitehead, A. C. Berg, W. Lo, P. Dollár, and R. B. Girshick, "Segment Anything," in *Proc. ICCV*, 2023, pp. 3992–4003.

[41] Z. Liu, Y. Lin, Y. Cao, H. Hu, Y. Wei, Z. Zhang, S. Lin, and B. Guo, "Swin Transformer: Hierarchical Vision Transformer using Shifted Windows," in *Proc. ICCV*, 2021, pp. 9992–10 002.

[42] A. Vaswani, N. Shazeer, N. Parmar, J. Uszkoreit, L. Jones, A. N. Gomez, L. Kaiser, and I. Polosukhin, "Attention is All you Need," in *Proc. NeurIPS*, 2017, pp. 5998–6008.

[43] J. Gehring, M. Auli, D. Grangier, D. Yarats, and Y. N. Dauphin, "Convolutional Sequence to Sequence Learning," in *Proc. ICML*, vol. 70, 2017, pp. 1243–1252.

[44] Y. Su, J. Deng, R. Sun, G. Lin, H. Su, and Q. Wu, "A Unified Transformer Framework for Group-Based Segmentation: Co-Segmentation, Co-Saliency Detection and Video Salient Object Detection," *T-MM*, vol. 26, pp. 313–325, 2024.

[45] F. Yang, H. Yang, J. Fu, H. Lu, and B. Guo, "Learning Texture Transformer Network for Image Super-Resolution," in *Proc. CVPR*, 2020, pp. 5790–5799.

[46] J. Hu, L. Shen, and G. Sun, "Squeeze-and-Excitation Networks," in *Proc. CVPR*, 2018, pp. 7132–7141.

[47] S. Woo, J. Park, J. Lee, and I. S. Kweon, "CBAM: Convolutional Block Attention Module," in *Proc. ECCV*, vol. 11211, 2018, pp. 3–19.

[48] T. Dai, J. Cai, Y. Zhang, S. Xia, and L. Zhang, "Second-Order Attention Network for Single Image Super-Resolution," in *Proc. CVPR*, 2019, pp. 11 065–11 074.

[49] F. Ding, G. Yang, J. Wu, D. Ding, J. Xv, G. Cheng, and X. Li, "High-Order Attention Networks for Medical Image Segmentation," in *Proc. MICCAI*, vol. 12261, 2020, pp. 253–262.

[50] B. Jiang, S. Luo, X. Wang, C. Li, and J. Tang, "AMatFormer: Efficient Feature Matching via Anchor Matching Transformer," *T-MM*, vol. 26, pp. 1504–1515, 2024.

[51] L. Ke, X. Li, M. Danelljan, Y. Tai, C. Tang, and F. Yu, "Prototypical Cross-Attention Networks for Multiple Object Tracking and Segmentation," in *Proc. NeurIPS*, 2021, pp. 1192–1203.

[52] J. Wang, S. Qian, J. Hu, and R. Hong, "Positive Unlabeled Fake News Detection via Multi-Modal Masked Transformer Network," *T-MM*, vol. 26, pp. 234–244, 2024.

[53] S. Ye, H. Wang, M. Tan, and F. Liu, "Recurrent Affine Transformation for Text-to-Image Synthesis," *T-MM*, vol. 26, pp. 462–473, 2024.

[54] Z. Xu, D. Wu, C. Yu, X. Chu, N. Sang, and C. Gao, "SCTNet: Single-Branch CNN with Transformer Semantic Information for Real-Time Segmentation," in *Proc. AAAI*, 2024, pp. 6378–6386.

[55] K. Grauman, A. Westbury, E. Byrne, Z. Chavis, A. Furnari, and et al., "Ego4D: Around the World in 3, 000 Hours of Egocentric Video," in *Proc. CVPR*, 2022, pp. 18 973–18 990.

[56] D. Damen, H. Doughty, G. M. Farinella, S. Fidler, A. Furnari, E. Kazakos, D. Moltisanti, J. Munro, T. Perrett, W. Price, and M. Wray, "Scaling Egocentric Vision: The EPIC-KITCHENS Dataset," *CoRR*, vol. abs/1804.02748, 2018.

[57] Y. Tang, Y. Tian, J. Lu, J. Feng, and J. Zhou, "Action Recognition in RGB-D Egocentric Videos," in *Proc. ICIP*, 2017, pp. 3410–3414.

[58] Y. Liu, Y. Liu, C. Jiang, K. Lyu, W. Wan, H. Shen, B. Liang, Z. Fu, H. Wang, and L. Yi, "HOI4D: A 4D Egocentric Dataset for Category-Level Human-Object Interaction," in *Proc. CVPR*, 2022, pp. 20 981–20 990.